Published in "Physica Status Solidi (a) 2009: doi: 10.1002/pssa.200925180"
which should be cited to refer to this work.

The effect of Pr_6O_{11} doping on superconducting properties of MgB_2

N. Ojha[1], V. K. Malik[2], C. Bernhard[2], and G. D. Varma*[,1]

[1] Department of Physics, Indian Institute of Technology, Roorkee 247667, India
[2] Department of Physics and Fribourg Centre for Nanomaterials-FriMat, University of Fribourg, Chemin du Musee, 1700 Fribourg, Switzerland

PACS 74.25.Ha, 74.25.Qt, 74.62.Dh, 74.70.Ad

* Corresponding author: e-mail gdvarfph@iitr.ernet.in, Phone: +91-1332-285353, Fax: +91-1332-273560

In this paper we report the effect of Pr_6O_{11} doping on the structural and superconducting properties of MgB_2. The bulk samples of Pr_6O_{11}-doped MgB_2 have been prepared with nominal compositions $Mg_{1-x}(Pr_6O_{11})_{x/6}B_2$ (where $x = 0.0$, 0.01, 0.02, 0.03, 0.04, and 0.05) via a standard solid-state reaction route by sintering in a reducing atmosphere of Ar/H_2. The superconducting transition temperature T_c of MgB_2 is found to decrease from 39 to 37 K when x increases from 0 to 0.05. The XRD results show the presence of MgO and PrB_6 secondary phases in the doped samples besides the main hexagonal phase of MgB_2. Improvement in critical current density (J_c), irreversibility field (H_{irr}), and upper critical field (H_{c2}) of doped samples has been observed. The J_c values at 10 and 20 K of the $x = 0.03$ sample are higher in the entire field region (0–6 T). At 10 K and 2 T field the J_c values of undoped and 0.03 Pr_6O_{11}-doped samples are 1.09×10^5 and 2.21×10^5 A/cm^2, respectively. Variations of H_{c2}, J_c, H_{irr}, and flux-pinning force (F_p) with doping concentrations have been studied in this paper and a correlation between these superconducting properties and structural characteristics of the samples has been found in the present work.

1 Introduction The discovery of superconductivity at 39 K in MgB_2 [1] offers the possibility of its wide engineering applications in a temperature range of 20–30 K, where the convential superconductors, such as Nb_3Sn and Nb-Ti alloy, cannot be used due to their low transition temperatures (T_c). Relatively high T_c, low cost, and lack of weak links are the salient features of MgB_2 superconductor that make it an important material for technological applications. The intragranular J_c and upper critical field (H_{c2}) of MgB_2 bulk have been reported to be higher than those of NbTi and Nb_3Sn superconductors [2, 3]. However, further enhancement of intergranular J_c has remained a topic of great scientific and technological interest. For example, the current path of MgB_2 is locally limited by the presence of secondary phases or lattice defects [4]. The intergranular J_c in polycrystalline MgB_2 is also limited by various factors, such as poor connectivity between superconducting grains and chemical heterogeneity at the grain boundaries [5]. Poor crystallinity as well as porosity within the MgB_2 matrix could act as a source of weak links [6, 7].

One of the major problems of MgB_2-based superconductivity technologies is that the J_c of MgB_2 materials is still not high enough to satisfy the industrial applications, especially under high magnetic fields. For practical applications, superconductors with high infield critical current density ($J_c(H)$), high irreversibility field (H_{irr}), and high upper critical field (H_{c2}) are required. MgB_2 has a high self-field J_c of 10^5–10^6 A/cm^2 at 4.2 K and 10^4–10^5 A/cm^2 at 20 K [8, 9]. However, the J_c falls in applied magnetic fields due to weak flux pinning and low H_{irr}. Significant research is being continued for the improvement of flux pinning and hence $J_c(H)$, H_{irr}, and H_{c2} of MgB_2. Chemical doping is an effective method for introducing flux pinners in a superconductor. Various nanoparticles and materials such as C, diamond, SiC, SiO_2, Ti, Zr, Fe, Ag, [10–17] and some organic compounds have been introduced in MgB_2. These dopants improved the flux pinning and $J_c(H)$ of MgB_2 to different extents. Nano-SiC and nano-C-doped MgB_2 attained infield J_c by more than one order of magnitude higher than that of undoped samples and their H_{irr} and H_{c2} values surpassed those of the existing LTS materials. Besides carbon, nanoparticles of many other materials like Ti, Zr, Y_2O_3, Dy_2O_3, Pr_6O_{11}, and Ho_2O_3 have been introduced as nano-pinning center, which significantly improve the pinning

behavior of MgB_2. Although dopants of different chemical and/or physical properties have been used, dopants with magnetic moment have rarely been used as pinning centers in MgB_2. Magnetic impurities usually have a stronger interaction with magnetic flux lines than nonmagnetic impurities and may exert a stronger force to trap the flux lines if they can be properly introduced into the superconducting matrix. Therefore, the pinning sites with strong magnetic moment may play an important role in further improving the pinning behavior of MgB_2. Magnetic elements such as Mn, Fe, Co, Ni [18–20] have been doped into MgB_2, but these magnetic elements often suppress the superconductivity and degrade its performance in a magnetic field due to the existence of a local magnetic field. Rare-earth elements (RE) often possess a strong magnetic moment, however, it has been seen that they do not much suppress the superconductivity of MgB_2 [21, 22]. A recent study by Chen et al. on 0.5–5.0 wt% Dy_2O_3-doped MgB_2 showed a significant enhancement in J_c in a low or medium field [22]. Cheng et al. [23] found no change in crystal structure, T_c, and H_{c2} but significant enhancement in J_c and H_{irr} in 0.1–10% Ho_2O_3-doped MgB_2. A similar study on Pr_6O_{11}-doped MgB_2 has shown improvement in J_c and H_{irr} for low-level doping (1 wt%) and degradation in performance of MgB_2 for higher-level doping [24]. Thus, the effect of doping of some rare-earth oxides on the superconducting and structural properties of MgB_2 has been studied. However, it has not been studied as extensively as for other elements. Therefore, more studies are required to explore the possible approaches of improving the performance of MgB_2 by rare-earth oxide doping. In this paper we report the effect of Pr_6O_{11} doping on the structural and superconducting properties of MgB_2. The bulk polycrystalline samples of Pr_6O_{11}-doped MgB_2 have been prepared with nominal compositions $Mg_{1-x}(Pr_6O_{11})_{x/6}B_2$ (where $x = 0.0$, 0.01, 0.02, 0.03, 0.04, and 0.05) using a standard solid-state reaction route. An improvement in J_c (H), H_{c2}, and H_{irr} of the doped samples has been observed in the present study.

2 Experimental A series of Pr_6O_{11}-doped MgB_2 samples with nominal compositions $Mg_{1-x}(Pr_6O_{11})_{x/6}B_2$ (where $x = 0.0$, 0.01, 0.02, 0.03, 0.04, and 0.05) were synthesized in a reducing atmosphere ($Ar + H_2$) via a standard solid-state reaction method. Appropriate amounts of Mg (99%), B (amorphous, 95–97%), and Pr_6O_{11} (99.9%) were mixed and pressed into rectangular pellets with the help of an hydraulic press. The pellets were sintered at 850 °C for 3 h in flowing Ar/H_2 (Ar: $H_2 = 9:1$) and subsequently furnace cooled down to room temperature. Henceforth, the MgB_2 samples synthesized with $x = 0.0$, 0.01, 0.02, 0.04, and 0.05 will be represented as MBP0, MBP1, MBP2, MBP3, MBP4, and MBP5, respectively. The structural and phase analyses of the samples were performed by an X-ray diffractometer (BRUKER D8) with CuK_α radiation. Microstructural and elemental analyses of the samples were done by FE-SEM (FEI Quanta 200 ESEM FEG) equipped with an Oxford Inca Energy Dispersive X-ray (EDAX) detector. The variation of resistance with temperature was studied with increasing magnetic field up to 8 T using a Quantum Design PPMS. Magnetization measurements of the samples were done using a Physical Properties Measurement System (PPMS Quantum Design-6000).

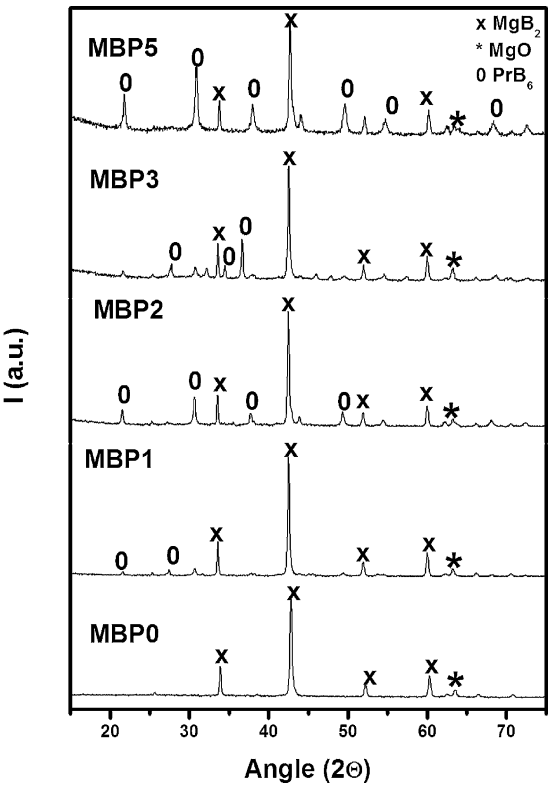

Figure 1 XRD patterns of Pr_6O_{11}-doped and undoped MgB_2 samples.

3 Results and discussion Figure 1 shows the X-ray diffraction (XRD) patterns of MgB_2 samples doped with different amounts of Pr_6O_{11}. The XRD results reveal the presence of mainly hexagonal phase of MgB_2 in all the samples. In addition to this, there are a few peaks corresponding to the secondary phases MgO and PrB_6. The peak intensities of PrB_6 phase increase with increasing doping concentration (x). This shows that the content of PrB_6 phase increases with increasing doping concentration of Pr_6O_{11} in the samples. We have estimated the volume fraction of MgO by taking the ratio of the peak intensity of MgO to the sum of the peak intensities of all other phases and the estimated values are 3.8, 3.6, 3.3, 4.4, and 3.0% in the samples MBP0, MBP1, MBP2, MBP3, and MBP5, respectively. There are no peaks corresponding to Mg, B, and Pr_6O_{11}. This suggests that added Pr_6O_{11} decomposed at reaction temperature and reacted with B to form PrB_6 and some of the Mg reacted with oxygen to form MgO. The formation of all the observed phases in the samples may be explained by the following equation:

$$(x/6)Pr_6O_{11} + (1 - x)Mg + 2B \rightarrow (1 - 3x)MgB_2 + 2x\ MgO + xPrB_6.$$

Table 1 Values of various parameters of Pr_6O_{11}-doped MgB_2 samples.

samples	a (Å)	c (Å)	strain	H_{c2} (T)	H_{irr} (T)		J_c (A/cm^2)		R_{298}/R_{onset}	A_F
					10 K	20 K	10 K, 5 T	20 K, 4 T		
MBP0	3.0803	3.5222	0.0056	12.02	6.06	4.30	4.86×10^2	1.89×10^2	3.38	0.14
MBP1	3.0789	3.5210	0.0102	12.77	6.33	5.65	2.75×10^3	2.46×10^3	3.48	0.17
MBP3	3.0759	3.5193	0.0123	14.51	6.38	5.72	3.82×10^3	5.74×10^3	3.21	0.23
MBP5	3.0741	3.5190	0.0326	15.92	5.88	5.45	4.45×10^3	3.70×10^3	2.81	0.28

As shown above, the MgO content in the samples does not increase systematically with increasing x, the actual numbers of moles of all three products, namely MgB_2, MgO, and PrB_6, in the samples are expected to be different from the values specified in the above equation. The XRD results show a decrease in lattice parameters a and c with increasing doping levels. However, the decrease in c is small as compared to that in a (see Table 1). As the ionic radius of Pr^{3+} (99 pm) is greater than the ionic radius of Mg^{2+} (86 pm), the observed decrease in lattice parameters with increasing Pr_6O_{11} content is not expected due to substitution of Pr at Mg site of MgB_2. We have estimated the strain value and crystallite size of the samples from the Williamson–Hall plot. The strain in the sample increases almost linearly with concentration of Pr_6O_{11} (Table 1). The linear increase in strain values with x is suggestive of a corresponding increase in lattice defect in the doped samples and possibly due to this there is a decrease in lattice parameters with increasing x. In the present case, however, the possibility of partial substitution of Pr at Mg sites of MgB_2 can not be completely ruled out. There may be partial substitution of Pr at Mg site as reported by Pan et al. [24], and a corresponding small increase in lattice parameters is suppressed by distortion produced in the lattice. Since we have synthesized the

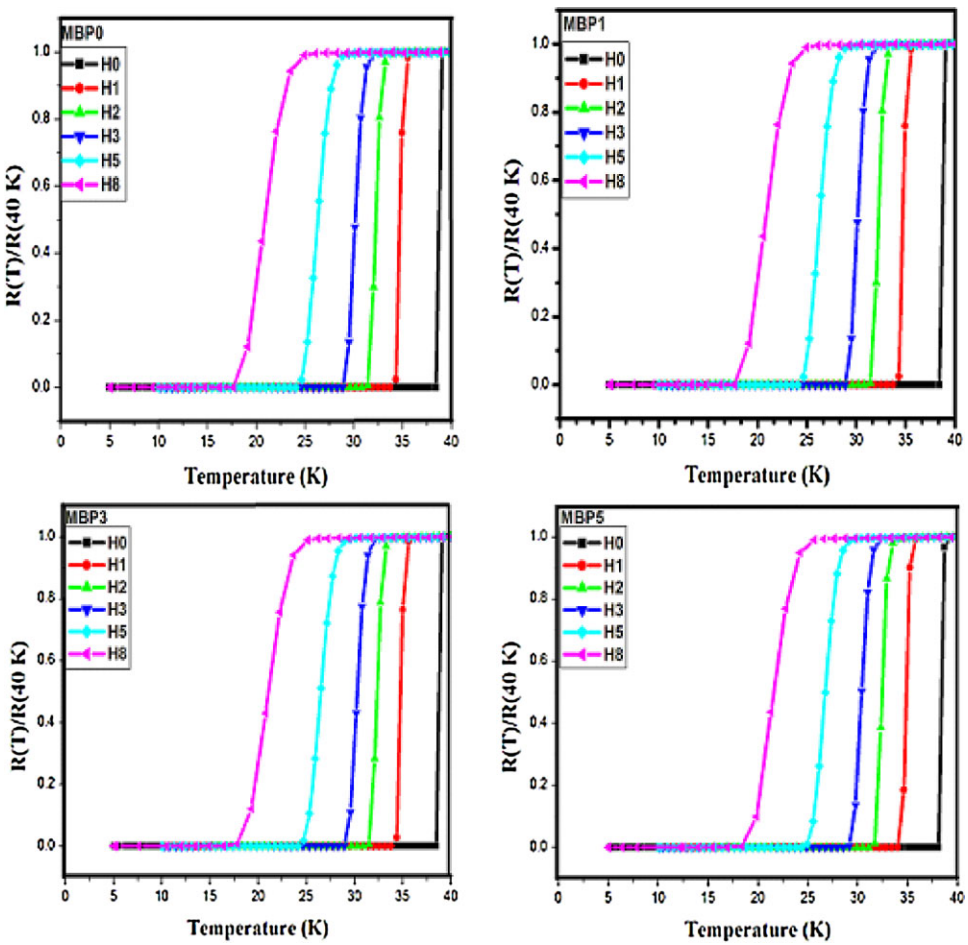

Figure 2 (online color at: www.pss-a.com) Superconductor transition zone of resistance versus temperature plots, at different applied fields (H), of Pr_6O_{11}-doped and undoped MgB_2 samples.

samples with nominal compositions $Mg_{1-x}(Pr_6O_{11})_{x/6}B_2$ ($x = 0.0$, 0.01, 0.02, 0.03, 0.04, and 0.05), we are decreasing the content of Mg with increasing Pr_6O_{11} concentration. Therefore, there is a possibility of Mg vacancies and the presence of oxygen in the lattice of doped samples. These lead to lattice defects and hence to an increase in the strain values. Earlier, Serquis et al. [25] also observed that strain linearly increases with a decrease in Mg occupancy in MgB_2 samples. In addition to Mg vacancies, nanoscale PrB_6 and MgO particles within MgB_2 grains may also be responsible for lattice distortion.

Figure 2 shows the *R–T* plots of the samples measured in different fields near the superconducting transitions. From the zero-field plots it is clear that the transition temperatures (T_c) vary from 39 to 37 K when doping concentration increases from $x = 0.0$ to 0.05. The same result is obtained from the *M–T* measurements (figure not shown here). The diamagnetic signal, however, has been found to decrease with increase in doping concentration. This result is in conformity with the XRD results that showed that the volume of secondary phases in the samples increases, i.e., superconducting volume decreases with the increase in doping concentration (x). In the present case small reduction in T_c with doping level is possibly due to the increase in strain value with doping concentration [25, 26] and partial substitution of Pr at Mg sites [24]. The residual resistivity ratio ($RRR = R_{295}/R_{onset}$) values continuously decreases with x, except for $x = 0.01$. This is due to the increase in the amount of impurity phases as doping concentration increases in the samples. These impurity phases can enhance the electron scattering, and hence the decreased RRR value [27].

Figure 3 shows the FE-SEM micrographs of the doped and undoped samples. From the FESEM micrographs it is also clear that the homogeneity of the microstructure is greater for the undoped sample, and it decreases with an increase of Pr_6O_{11} content in the sample. However, the connectivity of the grains becomes better in the samples of higher Pr_6O_{11} concentration. We have calculated the active area fraction (A_F) for all the samples using the formula $A_F = \Delta\rho_{ideal}/(\rho_{300\,K} - \rho_{40\,K})$, proposed by Rowell [28]. Here, $\Delta\rho_{ideal}$ is the ideal change in resistivity from 300 to 40 K for a fully connected sample and its value is taken to be 7.3 $\mu\Omega$ cm [29]. The calculated values of A_F are given in Table 1. It can be seen that the value of A_F increases, i.e. connectivity of the grains increases, with increasing x. The EDAX (figures not shown here) results confirm the presence of all the elements (which were taken in the starting compositions) in the samples.

Figure 4a and b show the *M–H* loops measured at 10 K and 20 K, respectively of the undoped and doped MgB_2 samples. Figure 4c and d show the field dependence of the critical current density J_c (H) of the samples estimated from the *M–H* loops (see Fig. 4a and b) measured at 10 K and 20 K, respectively. From the *M–H* loops J_c values have been estimated by using Bean's critical model [30]. From Fig. 4c it can be seen that at 10 K, with respect to the pure sample,

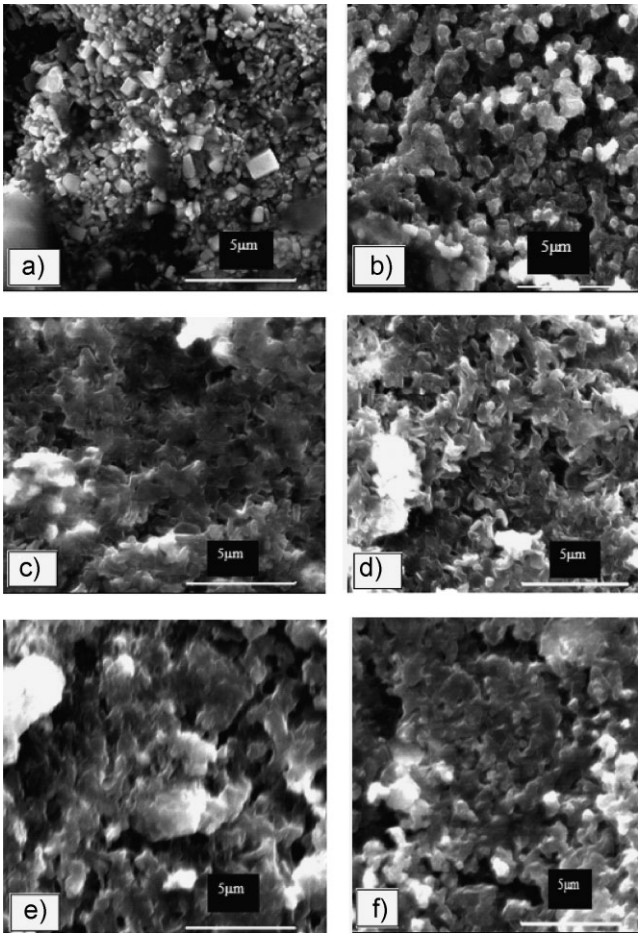

Figure 3 FE-SEM micrographs of samples MBP0 (a), MBP1 (b), MBP2 (c), MBP3 (d), MBP4 (e) and MBP5 (f).

samples MBP1 and MBP3 have higher critical current density in the entire field region (0–6.5 T), whereas sample MBP5 has a higher values of J_c in 3–5.5 T field range. For example, at 10 K and 2 T field the J_c values of samples MBP0, MBP1, MBP3, and MBP5 are 1.09×10^5, 1.71×10^5, 2.21×10^5, and 7.26×10^4 A/cm^2, respectively. A similar field dependence of J_c is observed at 20 K (see Fig. 4d). In the low-field region (<3 T) the field dependence of J_c of samples MBP1 and MBP3 is similar to the 1 and 3 wt% Pr_6O_{11}-doped MgB_2 of Pan et al. [24]. On the other hand, in the high-field region (3–5.5 T) we have seen substantial improvement in the J_c values of all doped samples as compared to the undoped sample. This result is quite different from the earlier results of Pan et al. where they have found improvement in J_c value of an only 1 wt% doped sample in the high-field region. In addition to this, our J_c values are higher than their J_c values at all applied fields [24]. We have determined the H_{irr} values of the doped and undoped samples from the closure of the *M–H* hysteresis loops with a criterion of $J_c = 100$ A/cm^2. The variations of H_{irr} at 10 and 20 K with doping level (x) are shown in Fig. 5a. At both temperatures the values of H_{irr} of samples MBP1 and MBP3 are higher as compared to sample MBP0. Thus, the Pr_6O_{11} doping effect on H_{irr} is the same as

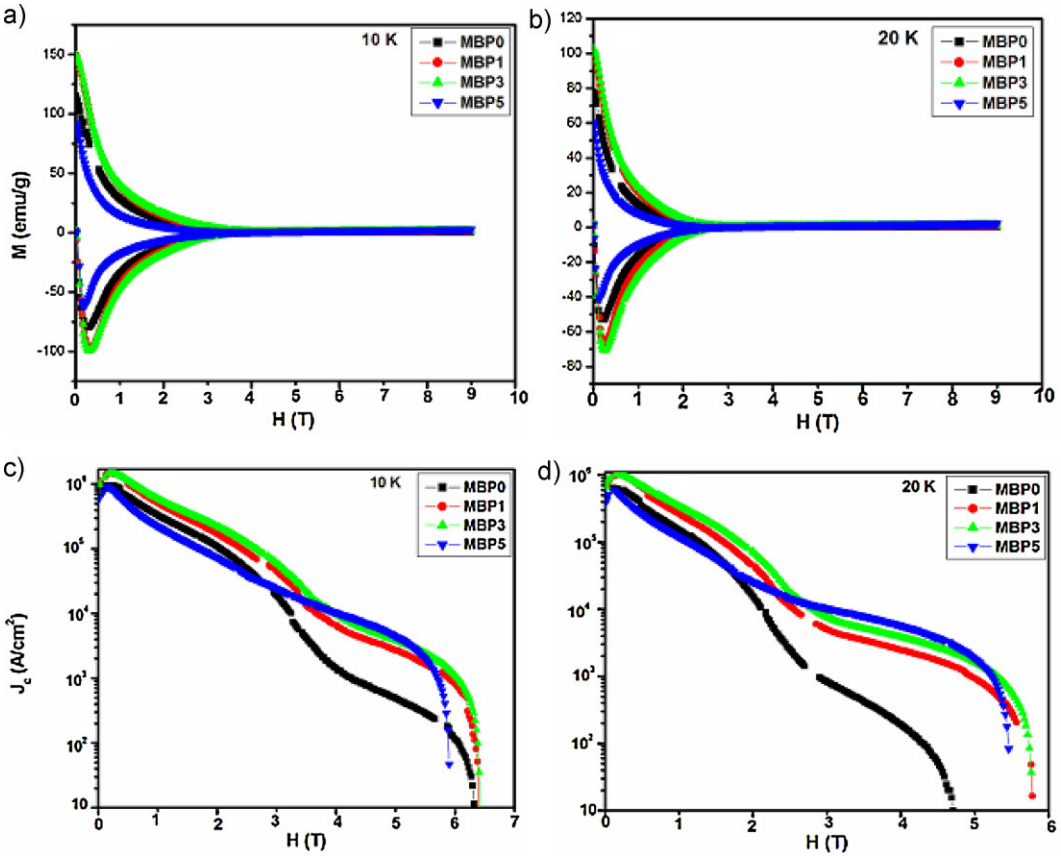

Figure 4 (online color at: www.pss-a.com) (a) and (b) The M–H loops of Pr_6O_{11}-doped MgB_2 samples measured at 10 and 20 K, respectively. (c) and (d) Variation of J_c with fields of Pr_6O_{11}-doped MgB_2 samples at 10 and 20 K, respectively.

on $J_c(H)$. The values of H_{irr} at 10 and 20 K of all samples are given in Table 1. Thus, the Pr_6O_{11} doping effect on H_{irr} is the same as on $J_c(H)$. The correlation between the full width at half-maximum (FWHM) of the (100) peak in the XRD patterns and the irreversibility fields of the samples studied in this work is shown in Fig. 5b. Both the FWHM of the (100) peak and H_{irr} vary with doping level in a very similar manner, i.e. when H_{irr} is high the (100) peak of the corresponding sample is significantly broadened and vice versa. Because the (100) peak of MgB_2 reflects the lattice constant of a honeycomb boron sheet in MgB_2 structure, the broadening of this peak may suggest the occurrence of some distortion of the sheet. Similar correlation between the FWHM of the (110) peak and H_{irr} has been observed by Yamamoto et al. [32]. The mechanism for the significant enhancement of critical current density may be related to the stronger pinning

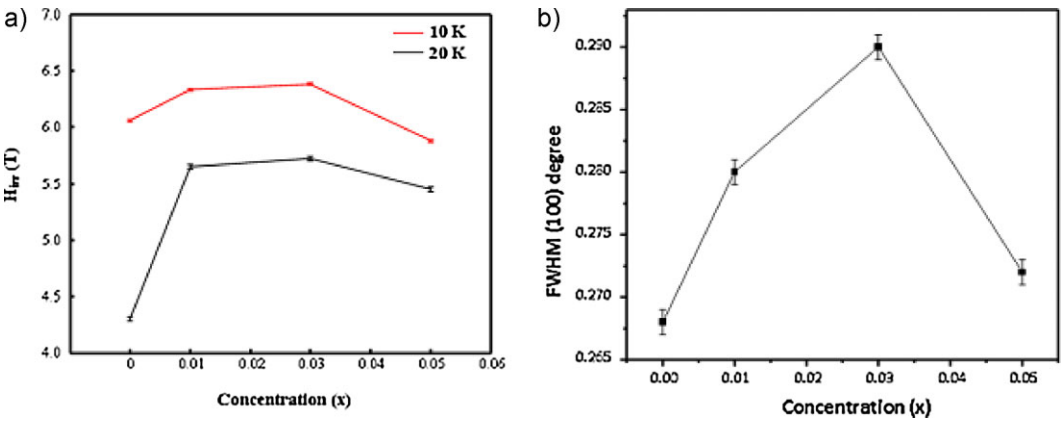

Figure 5 (online color at: www.pss-a.com) Variation of H_{irr} (a) and FWHM (b) with doping concentration of Pr_6O_{11} (x). The error bars at each data point represent the spread of the measured values of H_{irr} and FWHM of identical samples.

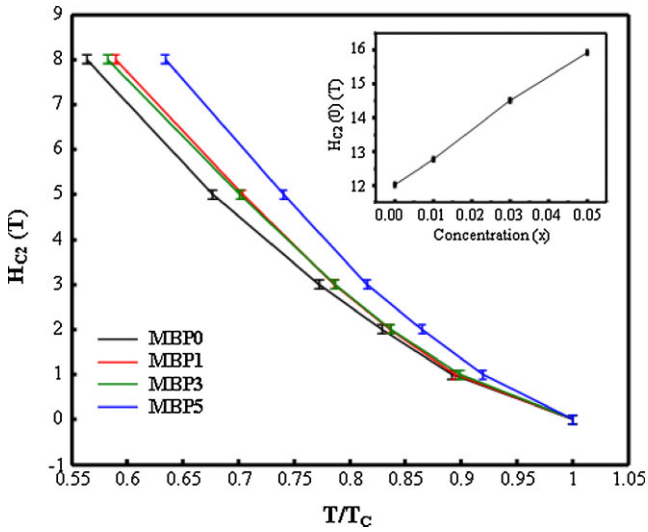

Figure 6 (online color at: www.pss-a.com) $H_{c2}(T)$ versus reduced temperature (T/T_c) plots of Pr_6O_{11}-doped and undoped MgB_2 samples. The error bars at each data point represent the spread of the measured values $H_{c2}(T)$ of identical samples.

force in Pr_6O_{11}-doped MgB_2. The decrease in J_c with further increase in doping level is due to the increased content of PrB_6 phase and defects in the samples. Therefore improved flux-pinning behavior in samples can be mainly due to secondary phases and defects.

The upper critical fields ($H_{c2}(T)$) at various temperatures have been calculated from the resistive transitions using the criteria 90% of $R(T_c)$ [33]. The variations of $H_{c2}(T)$ with respect to reduced temperature for each composition are shown in Fig. 6. The values of $H_{c2}(0)$ for the doped and undoped samples have been calculated using the formula $H_{c2}(0) = 0.693T_c(dH_{c2}/dT)$ based on the Werthamer–Helfand–Hohenberg model [34]. The inset of Fig. 6 shows the variation of $H_{c2}(0)$ with composition x. It can be seen that the value of $H_{c2}(0)$ increases with increasing doping level in the sample (see Table 1). It has been reported that the enhancement in the upper critical field results from the reduction of the mean-free path of the charge carriers and the corresponding reduction of the coherence length [35]. In the present study we calculated the coherence length for the undoped and doped samples using the relation $\xi(0) = (\Phi(0)/2\pi H_{c2}(0))^{0.5}$. The values of coherence length are 4.8 nm for MBP0 and 4.5 nm for MBP5. The enhancement in H_{c2} observed in the present case is possibly due to lattice distortion created through Pr_6O_{11} doping leading to enhanced impurity scattering.

To confirm the fact that improvement in J_c of MgB_2 in the high-field region is due to improved flux-pinning behavior through Pr_6O_{11} doping, we have calculated the flux-pinning force (F_p) at 10 and 20 K, for each composition by using the relation $F_p = J_c(H) \times H(T)$ [36, 37]. The variation of normalized flux pinning force ($F_p/F_{p,max}$) with magnetic field for each composition is shown in Fig. 7. This figure depicts a significant improvement in pinning force in the doped samples as compared to undoped sample. In the high-field region (3–6 T), the values of normalized pinning force of sample MBP5 are higher as compared to other doped samples (see Fig. 7). On the other hand, in the low-field region (<3 T), the values of normalized pinning force of MBP3 are higher as compared to other samples. Thus, we find a correlation between J_c–H and $F_p/F_{p,max} - H$ plots. Therefore, it can be concluded that improvement in $J_c(H)$ of the doped samples is due to enhancement of the flux-pinning force. In order to study the magnetic properties of impurity phases we measured the M–H curves of MBP0 and MBP5 samples at room temperature by VSM. From this measurement we find that the MBP0 sample shows diamagnetic behavior, possibly due to the presence of trace amount of MgO in the sample, and the MBP5 sample exhibits paramagnetic behavior at room temperature. After subtracting the magnetization values at each field of the MBP0 sample from the corresponding values of the MBP5 sample we got the magnetization value of PrB_6 secondary phase. From this we came to the conclusion that the secondary PrB_6 phase is paramagnetic at room temperature. The presence of PrB_6 (magnetic impurities) in the doped samples may provide a stronger attraction force to flux lines than the nonmagnetic impurities and hence enhance the flux-pinning effect in

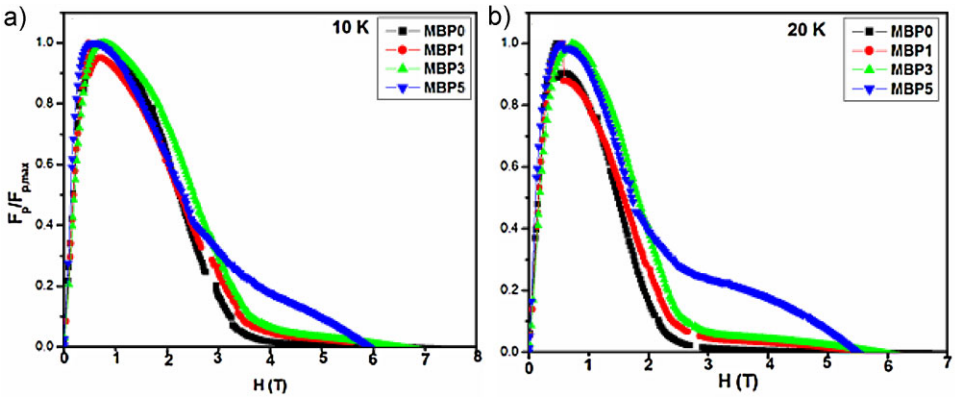

Figure 7 (online color at: www.pss-a.com) Normalized flux-pinning force versus field (H) plots of Pr_6O_{11}-doped MgB_2 samples.

MgB_2 without much affecting its T_c. The impurity phases PrB_6 and MgO are likely to be distributed at the grain boundaries and within the grains of MgB_2. Chen et al. [22] have shown that in Dy_2O_3-added MgB_2 samples nanoscale precipitates of DyB_4 and MgO within the MgB_2 grains act as effective pinning centers. Similarly, in the present samples the nanoscale PrB_6 and MgO within the grains are expected to act as effective pinning centers. We have seen above that the sample MBP3 showed the highest value of $J_c(H)$ of all the samples studied. This may be explained on the basis of MgO content in the samples. From the XRD results we have seen the highest MgO content in the sample MBP3. Kováč et al. [31] reported that well-distributed small-sized MgO particles improve flux pinning in samples. Therefore, in the present case enhanced flux pinning is expected in the sample MBP3 which leads to its highest $J_c(H)$ value. From the XRD results we have seen an increase in strain with increasing doping level, possibly due to Mg vacancies and the presence of oxygen in the MgB_2 lattice. This shows that lattice distortions in the samples increase with increasing doping level. These distortions, which are expected mainly in the form of point defects, may also act as flux-pinning centers, leading to improvement in $J_c(H)$.

4 Summary In summary, the Pr_6O_{11}-doped MgB_2 samples with nominal compositions $Mg_{1-x}(Pr_6O_{11})_{x/6}B_2$ has been prepared by a solid-state reaction method at ambient pressure. We have seen improvement in J_c, H_{irr}, and H_{c2} of the doped samples as compared to undoped samples. It has been conjectured that the presence of PrB_6 (magnetic impurity) and MgO at grain boundaries and within the grains, and lattice distortion, provide a stronger pinning force leading to improvement in $J_c(H)$. The MBP3 sample has highest values of J_c in the entire applied field region (0–6 T). This is due to the highest MgO content in this sample that enhances its flux-pinning property.

Acknowledgements This work was supported by M.H.R.D. (Govt. of India), C.S.I.R. (Govt. of India) and by the Schweizer Nationalfonds (SNF) by grant 200020-119784. The authors are grateful to Dr. Rajiv Rawat (UGC-DAE CSR, Indore) for doing the *R–T* measurements in magnetic fields.

References

[1] J. Nagamatsu, N. Nakagawa, T. Muranaka, Y. Zenitani, and J. Akimitsu, Nature **410**, 63 (2001).
[2] B. J. Senkowich, J. E. Giencke, S. Patnaik, C. B. Eom, E. E. Hellstrom, and D. C. Larbalestier, Appl. Phys. Lett. **86**, 202502 (2005).
[3] M. D. Sumption, M. Bhatia, X. Fu, M. Rindfleisch, M. Tomsic, and E. W. Collings, Supercond. Sci. Technol. **18**, 730 (2005).
[4] S. Hata, T. Yoshidom, H. Sosiati, Y. Tomokiyo, N. Kuwano, A. Matsumoto, H. Kitaguchi, and H. Kumakura, Supercond. Sci. Technol. **19**, 161 (2006).
[5] H. Fang, Y. Y. Xue, Y. X. Zhou, A. Baikalov, and K. Salama, Supercond. Sci. Technol. **17**, L27 (2004).
[6] C. F. Liu, G. Yan, S. J. Du, W. Xi, Y. Feng, P. X. Zhang, X. Z. Wu, and L. Zhou, Physica C **386**, 603 (2003).
[7] D. Eyidi, O. Eibl, T. Wenzel, K. G. Nickel, M. Giovannini, and A. Saccone, Micron **34**, 85 (2003).
[8] C. Buzea and K. Robbie, Supercond. Sci. Technol. **18**, R1 (2005).
[9] K. Vinod, R. G. Abhilash Kumar, and U. Syamaprasad, Supercond. Sci. Technol. **20**, R1 (2007).
[10] Y. W. Ma, X. P. Zhang, J. Nishijima, K. Watanabe, S. Awaji, and X. D. Bai, Appl. Phys. Lett. **88**, 072502 (2006).
[11] C. H. Cheng, H. Zhang, Y. Zhao, Y. Feng, F. Ruix, P. Munroe, H. M. Zeng, N. Koshizuka, and M. Murakami, Supercond. Sci. Technol. **16**, 1182 (2003).
[12] S. C. Yan, G. Yan, Y. F. Lu, and L. Zhou, Supercond. Sci. Technol. **20**, 549 (2007).
[13] X. F. Rui, Y. Zhao, Y. Y. Xu, L. Zhang, X. F. Sun, Y. Z. Wang, and H. Zhang, Supercond. Sci. Technol. **17**, 689 (2004).
[14] Y. X. Sun, D. L. Yu, Z. Y. Liu, T. S. Wang, J. L. He, J. Y. Xiang, D. N. Zheng, S. Choi, and T. Kiyoshi, Supercond. Sci. Technol. **20**, 261 (2007).
[15] Y. Feng, Y. Zhao, A. K. Pradhan, C. H. Cheng, J. K. P. Yau, L. Zhou, N. Koshizuka, and M. Murakami, J. Appl. Phys. **92**, 2614 (2002).
[16] E. Kuzmann, Z. Homonnay, Z. Klencsar, M. Kuhberger, A. Vertes, and G. Gritzner, Supercond. Sci. Technol. **15**, 1479 (2002).
[17] S. Soltanian, X. L. Wang, J. Horvat, A. H. Li, H. K. Liu, and S. X. Dou, Physica C **382**, 187 (2002).
[18] M. Kuhberger and G. Gritzner, Phys. C **370**, 29 (2002).
[19] H. Kitaguchi and H. Kumakura, Supercond. Sci. Technol **18**, S284 (2005).
[20] C. H. Cheng, Y. Zhao, X. T. Zhu, J. Nowotny, C. C. Sorrell, T. Finlayson, and H. Zhang, Physica C **386**, 588 (2003).
[21] J. Wang, Y. Bugoslavsky, A. Berenov, L. Cowey, A. D. Caplin, L. F. Cohen, J. L. M. M. Driscoll, L. D. Cooley, X. Song, and D. C. Larbalestier, Appl. Phys. Lett. **89**, 2026 (2002).
[22] S. K. Chen, M. Wei, and J. L. M. M. Driscoll, Appl. Phys. Lett. **88**, 192512 (2006).
[23] C. Cheng and Y. Zhao, Appl. Phys. Lett. **89**, 252501 (2006).
[24] X. F. Pan, T. M. Shen, G. Li, C. H. Cheng, and Y. Zhao, Phys. Status Solidi **204**, 1555 (2007).
[25] A. Serquis, Y. T. Zhu, E. J. Peterson, J. Y. Coulter, D. E. Peterson, and F. M. Mueller, Appl. Phys. Lett. **79**, 4399 (2001).
[26] Y. Zhu, L. Wu, V. Volkov, Q. Li, G. Gu, A. R. Moodenbaugh, M. Malac, M. Suenaga, and J. Tranquada, Physica C **356**, 239 (2001).
[27] A. Vajpayee, V. P. S. Awana, G. L. Bhalla, and H. Kishan, Supercond. Sci. Technol. **19**, 125708 (2008).
[28] J. M. Rowell, Supercond. Sci. Technol. **16**, R17 (2003).
[29] C. Canfield, D. K. Finnemore, S. L. Bud'ko, J. E. Ostenson, G. Lapertot, C. E. Cunningham, and C. Petrovic, Phys. Rev. Lett. **86**, 2423 (2001).
[30] C. P. Beans, Rev. Mod. Phys. **36**, 31 (1964).
[31] P. Kováč, I. Hušek, T. Melišek, J. C. Grivel, W. Pachla, V. Štrbík, R. Diduszko, J. Homeyer, and N. H. Andersen, Supercond. Sci. Technol. **17**, L41 (2004).
[32] A. Yamamoto, J. Shimoyama, S. Ueda, Y. Katsura, I. Iwayama, S. Horii, and K. Kishio, Appl. Phys. Lett. **86**, 212502 (2005).

[33] S. Patnaik, L. D. Cooley, A. Gurevich, A. A. Polyanskii, J. Jiang, X. Y. Cai, A. A. Squitieri, M. T. Naus, M. K. Lee, J. H. Choi, L. Belenky, S. D. Bu, J. Letteri, X. Song, D. G. Schlom, S. E. Babcock, C. B. Eom, E. E. Hellstrom, and D. C. Larbalestier, Supercond. Sci. Technol. **14**, 315 (2001).
[34] N. R. Werthamer, E. Helfand, and P. C. Hohenberg, Phys. Rev. **147**, 288 (1966).
[35] N. Horhager, M. Eisterer, H. W. Weber, T. Prikhna, T. Tajima, and V. F. Nesterenko, J. Phys. Conf. Series **43**, 500 (2006).
[36] E. Matinez, P. Mikheenko, M. Martinez-lopez, A. Millan, A. Bevan, and J. S. Abell, Phys. Rev. B. **75**, 134515(2007).
[37] T. M. Shen, G. Li, C. H. Cheng, and Y. Zhao, Supercond. Sci. Technol. **19**, 1219 (2006).